Immunology:

Structural Basis for Complement Evasion by Lyme Disease Pathogen *Borrelia burgdorferi*

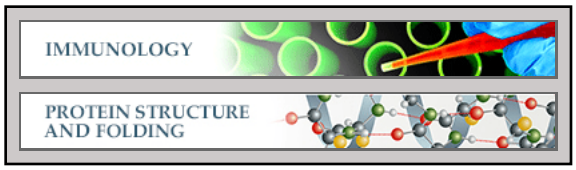

Arnab Bhattacharjee, Jesper S. Oeemig, Robert Kolodziejczyk, Taru Meri, Tommi Kajander, Markus J. Lehtinen, Hideo Iwaï, T. Sakari Jokiranta and Adrian Goldman

J. Biol. Chem. 2013, 288:18685-18695.
doi: 10.1074/jbc.M113.459040 originally published online May 8, 2013

THE JOURNAL OF BIOLOGICAL CHEMISTRY VOL. 288, NO. 26, pp. 18685–18695, June 28, 2013

Structural Basis for Complement Evasion by Lyme Disease Pathogen *Borrelia burgdorferi*

Received for publication, February 12, 2013, and in revised form, April 28, 2013 Published, JBC Papers in Press, May 8, 2013, DOI 10.1074/jbc.M113.459040

Arnab Bhattacharjee[‡§], Jesper S. Oeemig[§1,2], Robert Kolodziejczyk[§¶1], Taru Meri[‡¶], Tommi Kajander[§3], Markus J. Lehtinen[‡], Hideo Iwaï[§4], T. Sakari Jokiranta[‡5,6], and Adrian Goldman[§¶5,7]

From the [‡]Haartman Institute, Department of Bacteriology and Immunology, and Research Programs Unit, Immunobiology, the [§]Institute of Biotechnology, and the [¶]Department of Biosciences, Division of Biochemistry and Biotechnology, University of Helsinki, FIN-00014 Helsinki, Finland

Background: *Borrelia burgdorferi* OspE protein recruits complement regulator FH onto the bacteria for immune evasion.
Results: We solved the structure of OspE and the OspE·FH complex by NMR and x-ray crystallography.
Conclusion: The OspE·FH structure shows how *Borrelia* evade complement attack by mimicking how host cells protect themselves.
Significance: This explains how the bacteria survive in the host and facilitates vaccine design against borreliosis.

Borrelia burgdorferi **spirochetes that cause Lyme borreliosis survive for a long time in human serum because they successfully evade the complement system, an important arm of innate immunity. The outer surface protein E (OspE) of *B. burgdorferi* is needed for this because it recruits complement regulator factor H (FH) onto the bacterial surface to evade complement-mediated cell lysis. To understand this process at the molecular level, we used a structural approach. First, we solved the solution structure of OspE by NMR, revealing a fold that has not been seen before in proteins involved in complement regulation. Next, we solved the x-ray structure of the complex between OspE and the FH C-terminal domains 19 and 20 (FH19-20) at 2.83 Å resolution. The structure shows that OspE binds FH19-20 in a way similar to, but not identical with, that used by endothelial cells to bind FH via glycosaminoglycans. The observed interaction of OspE with FH19-20 allows the full function of FH in down-regulation of complement activation on the bacteria. This reveals the molecular basis for how *B. burgdorferi* evades innate immunity and suggests how OspE could be used as a potential vaccine antigen.**

The number of patients with Lyme disease, also known as Lyme borreliosis, is increasing in the United States and Europe (1), making this disease one of the major emerging arthropod-borne infections in the world (2, 3). The disease is caused by the three main genospecies from the *Borrelia burgdorferi* sensu lato group: *B. burgdorferi* sensu stricto, *Borrelia afzelii*, and *Borrelia garinii* (4). These spirochetes are transmitted to human skin from the mid-gut of *Ixodes* sp. *ticks* if the feeding time is long enough (5). The earliest manifestation of the infection is erythema chronicum migrans, a slowly expanding skin rash around the tick bite, whereas the variable later stage manifestations are from organs where the bacteria have spread from skin mainly via blood circulation (6). These manifestations include arthritis and central nervous system disorders, depending on the *Borrelia* genospecies involved in the infection; *B. burgdorferi* sensu stricto is relatively arthrotropic, whereas *B. garinii* is generally neurotropic (7).

The Lyme *Borrelia* can survive for years inside the human body without evoking an efficient immune attack by the host. This is widely attributed to the powerful tools that these spirochetes use to evade host innate and acquired immune responses. Efficient down-regulation of complement, a major innate immune system of the host, on the surface of *Borrelia* is essential for survival of these pathogens in human serum and therefore central in their immune evasion (8, 9). Complement is an ancient arm of innate immunity composed of a group of plasma proteins activated by three initiation pathways. The alternative pathway initiates a non-selective attack against all surfaces in contact with host plasma and thus is responsible for the wide spectrum attack mounted by innate immunity. If a surface is unprotected, the initial attack leads to amplified activation, which results in enhanced phagocytosis, formation of lytic membrane pores, and release of chemotactic peptides (10).

Down-regulation of complement on *Borrelia* is mediated by recruitment of host complement regulator factor H (FH)[8] onto

[S] This article contains supplemental Figs. 1–8.
The atomic coordinates and structure factors (codes 2M4F and 4J38) have been deposited in the Protein Data Bank (http://wwpdb.org/).
The OspE resonance assignment has been deposited to BMRB with accession number 19001.

[1] Both authors contributed equally to this work.
[2] Supported by the National Graduate School in Informational and Structural Biology graduate school.
[3] Supported by the Sigrid Jusélius Foundation and Academy of Finland Grant 251700.
[4] Supported by the Sigrid Jusélius Foundation and Academy of Finland Grants 131413 and 137995.
[5] Both authors contributed equally to this work.
[6] Supported by the Sigrid Jusélius Foundation and Academy of Finland Grants 128646, 255922, and 259793. To whom correspondence may be addressed: Haartman Institute, Haartmaninkatu 3, University of Helsinki, FIN-00014 Helsinki, Finland. Tel.: 358-9-1911; Fax: 358-9-191-26382; E-mail: Sakari.Jokiranta@helsinki.fi.
[7] Supported by the Sigrid Jusélius Foundation and Academy of Finland Grant 1252206. To whom correspondence may be addressed: Department of Biosciences, Division of Biochemistry and Biotechnology, Viikinkaari 1, University of Helsinki, FIN-00014 Helsinki, Finland. Tel.: 358-9-1911; Fax: 358-9-191-59940; E-mail: Adrian.Goldman@helsinki.fi.

[8] The abbreviations used are: FH, factor H; OspE and -A, outer surface protein E and A, respectively; HSQC, heteronuclear single quantum correlation; TROSY, transverse relaxation optimized spectroscopy; SALP, SsgA-like protein; r.m.s.d., root mean square deviation.

the cell surface by two outer surface proteins, OspE (also known as the *B. burgdorferi* complement regulator-acquiring surface protein 3, BbCRASP-3)) and BbCRASP-1 (11–13). These proteins, unlike some other borrelial FH-binding proteins, are expressed on *Borrelia in vitro* at human body temperature and *in vivo* in a mammalian host (14). Practically all patient-derived *B. burgdorferi* sensu stricto strains have genes encoding OspE and/or one or more of the highly homologous FH-binding Erp proteins (the Erp paralogs) (15). OspE has been shown to be important for survival of *B. burgdorferi* sensu stricto and *B. garinii* because addition of fluid phase recombinant OspE to serum (blocking binding of FH onto the bacterial surface) results in impaired bacterial survival (13).

FH is a 150-kDa plasma glycoprotein made up of 20 globular complement control protein modules (CCP modules), each consisting of ~60 amino acids. It is essential for keeping complement activation under control both in plasma and on host cells. The central role of FH-mediated regulation on host cells is clearly demonstrated by impaired regulation due to mutations in domains 19–20, leading to a severe systemic disease, atypical hemolytic uremic syndrome (16, 17). Although FH domains 1–4 mediate the regulatory activity (18), we and others have recently shown that the recognition of host cells results from joint binding of domain 20 to cell surface glycosaminoglycans (or heparin) and domain 19 to the main complement opsonin C3b (19, 20).

Borrelia are not the only pathogenic microbes able to bind human FH to protect themselves against the host complement attack (21–23). Two regions on FH mediate binding to practically all FH-binding pathogens, one in domains 6 and 7 and another in domains 19 and 20 (FH19-20) (24–29). Both of these regions also contain glycosylaminoglycan-binding sites (30, 31). *B. burgdorferi* acquires FH via FH19-20 using the surface lipoprotein OspE (27), but it is not known which part of OspE is responsible for FH binding because both N- and C-terminal OspE truncations abolish FH binding (15). To date, there are no bacterial surface protein structures solved in complex with FH19-20 and only one structure of a bacterial protein bound to FH domains 6 and 7 (32).

Currently there is no vaccine available for Lyme borreliosis because the previously used outer surface lipoprotein A (OspA)-based vaccine was withdrawn from the market a decade ago due to serious side effects (33). A vaccine would, however, be highly valuable in clinical practice. Because the recent advancement in developing a vaccine against another difficult and important bacterial target, group B meningococcus, is based on a *Neisseria meningitidis* protein that binds host FH, we thought that a similar strategy might work with *Borrelia*. We therefore decided to determine the structural basis of host FH binding by *B. burgdorferi*. We used both NMR and x-ray crystallography together with further biophysical analyses and mutagenesis data described elsewhere (34) to characterize the interaction between OspE and domains 19 and 20 of FH. This is the first structure of a microbial protein that binds FH20. The OspE structure in solution and in complex with FH19-20 reveals how *B. burgdorferi* evades complement attack and is therefore able to cause human infection, paving the way to develop OspE as a vaccine candidate.

EXPERIMENTAL PROCEDURES

Expression of Proteins and OspE·FH19-20 Complex Formation—Cloning and purification have been described previously for wild type (35) and mutant FH19-20 proteins (36, 37). For crystallography, OspE was cloned, expressed, and purified as described earlier (13). For NMR, OspE (residues 21–171) was cloned into the pHYRSF53-36 vector between the BamHI and HindIII sites with an N-terminal hexahistidine tag and a yeast Smt3 domain (38). The construct was expressed in *E. coli* ER2566 strain grown in M9 medium containing $^{15}NH_4Cl$ and D-[$^{13}C_6$]glucose as sole nitrogen and carbon sources, respectively. Cells were grown at 310 K, and at A_{600} ~0.5, protein expression was induced by the addition of 0.5 mM isopropyl β-D-1-thiogalactopyranoside. After 4 h of protein expression, cells were harvested by centrifugation at 9,400 × *g* at 277 K for 10 min. The cell pellet was resuspended in 50 mM sodium phosphate buffer (pH 8.0) with 300 mM NaCl and flash-frozen in liquid nitrogen until protein purification. After being thawed, the cells were sonicated for 15 min (60% of total power) using a rod type sonicator on an ice bath for protein release. After centrifugation (45 min, 42,500 × *g*), the supernatant was loaded onto a 5-ml HisTrap FF column (GE Healthcare), and the bound protein was eluted with an imidazole gradient (25 ml gradient of 30–250 mM imidazole at 2 ml/min). Fractions containing His_6-Smt3-OspE were digested with yeast ubiquitin-like-protein protease (Ulp1) in PBS containing 1 mM DTT at 298 K for 4 h (20 μl of Ulp1 for each 20 ml of the OspE-containing solution). The digested sample was then loaded on a 5-ml HisTrap FF column to remove His_6-Smt3 and His_6-Ulp1, and OspE was collected in the flow-through. After dialysis (overnight against 2 liters of 20 mM sodium phosphate, pH 6.0), the purity of OspE in SDS-PAGE was >95% (supplemental Fig. 1*a*).

Light Scattering and Size Exclusion Chromatography Analysis—We used size exclusion chromatography coupled with multiangle light scattering to find the optimal proportions of FH19-20 and OspE to form the complex in solution (supplemental Fig. 1*b*). The proteins alone and their mixtures at two different apparent molar ratios (1:1 and 1:1.25) were run over a Superdex200 column attached to HPLC equipment (Shimadzu). A MiniDAWN TREOS light-scattering detector and Optilab rEX refractive index detector together with ASTRA version 5.3.4.20 software (Wyatt Technology Corp.) were used to calculate masses of proteins and complexes eluted from the column. A size exclusion analysis of OspE and FH19-20 alone and the OspE·FH19-20 complex was done by running the preparates through a Superdex200 column attached to an ÄKTA purifier HPLC system (GE Healthcare) (Fig. 2*a*). All samples were eluted in PBS at a 0.5 ml/min flow rate at 22 °C.

NMR Spectroscopy and Resonance Assignment of OspE—All NMR measurements were performed on Varian Inova 600-MHz or Varian Inova 800-MHz spectrometers, both equipped with a triple resonance cold probe. For structure determination of OspE, measurements were performed at 298 K on a 1 mM ^{15}N- and ^{13}C-labeled protein sample in 20 mM phosphate buffer (pH 6.0). Sequence-specific resonance assignment was based on a series of standard spectra: ^{15}N heteronuclear single quantum correlation (HSQC), aliphatic constant time ^{13}C HSQC,

HNCA, HNcoCA, HNCACB, CBCAcoNH, HNcaCO, HNCO, HBHAcoNH, ^{15}N-edited total correlation spectroscopy (TOCSY) with 50-ms mixing time, CCCcoNH, HcCH COSY, and HcCH TOCSY with 50-ms mixing time. Aromatic rings were assigned based on (HB)CB(CD)HD, (HB)CB(CDCE)-HE, and aromatic constant time ^{13}C HSQC. For structure calculation, ^{15}N-edited NOE NOESY-HSQC and ^{13}C-edited NOESY-HSQC were recorded with 80-ms mixing time at a ^{1}H frequency of 800 MHz (Table 1). All spectra were processed using NMRPipe (39), and specific resonance assignment was performed using the CCPNMR analysis suite software version 2.2.1 (40). The chemical shifts and the unassigned NOE peak lists were used as inputs for NMR structure calculation with the program CYANA version 3.0 (41, 42). Twenty structures with the lowest CYANA target functions were selected for energy refinement in a 5 Å water shell using the AMBER force field. Ramachandran plot was generated using PROCHECK-NMR (43), and it indicated that 81.9% of the residues were in the most favored and 18.1% in the additional allowed regions.

All relaxation measurements were performed at a ^{1}H frequency of 600 MHz. T_1 relaxation rates were determined using the T_1 relaxation times of 10, 20, 30, 40, 50, 60, 70, 90, 110, 130, 150, and 210 ms. T_2 relaxation rates were determined using a Carr-Purcell-Meiboom-Gill sequence (CPMG)-based pulse sequence with a 1.3-ms refocusing interval, and the used T_2 relaxation times were 10, 30, 50, 70, 90, 110, 130, and 150 ms (44). Heteronuclear ^{15}N{^{1}H}-NOEs were determined by recording [^{1}H,^{15}N] HSQC spectra with and without 3.5 s of ^{1}H saturation (supplemental Fig. 2). Peak intensities from the recorded spectra were used for data analysis.

Monitoring OspE and FH19-20 Interaction by NMR Spectroscopy—The ^{15}N-labeled OspE was titrated with unlabeled FH19-20, and monitoring the [^{1}H,^{15}N] transverse relaxation optimized spectroscopy (TROSY) spectra indicated that OspE and FH19-20 formed a complex. Backbone resonance assignments of the OspE in complex with FH19-20 were performed on 0.3 mM ^{15}N- and ^{13}C-labeled OspE saturated with FH19-20, using TROSY variants of HNCA, HN(CO)CA, HNCO, and HN(CA)CO spectra recorded at 308 K. The chemical shift differences between free OspE and OspE·FH19-20 complex were calculated for each residue using the equation,

$$\Delta\delta_{ave}[ppm] = ((\Delta\delta_{HN}[ppm])^2 + 0.17 \cdot (\Delta\delta_{N}[ppm])^2)^{0.5} \quad \text{(Eq. 1)}$$

where $\Delta\delta_{HN}$ and $\Delta\delta_{N}$ are the chemical shift differences for backbone H^N and N atoms (supplemental Fig. 3).

Crystallizing the OspE·FH19-20 Complex and Solving Its Structure—FH19-20 tends to crystallize as a homotetramer (35); therefore, we used FH19-20 with mutations D1119G and Q1139A to prevent this happening, as we have done before (20). The FH19-20$_{D1119G,Q1139A}$ protein has similar binding affinity for OspE as the wild type FH19-20 (mean IC_{50} of 0.55 *versus* 0.42 μM) (supplemental Fig. 4). The FH19-20$_{D1119G,Q1139A}$·OspE complex was crystallized at 293 K from sitting drops in the presence of 2 M ammonium sulfate, 0.1 M citric acid, and 0.2 M sodium chloride at pH 5.5. Crystals appeared within 4 days and were cryoprotected in the mother liquor supplemented with 25% glycerol. The diffraction data (to 2.83 Å) were collected at the ESRF ID14-4 beam line at 100 K on a Q315r ADSC CCD detector at 0.97372 Å. The data were indexed and scaled using XDS (45). The structure of the OspE·FH19-20 complex was initially solved by structure-optimized molecular replacement with Rosetta (46). A molecular replacement solution was obtained using the wild type FH19-20 structure (Protein Data Bank code 2G7I) (35) and a truncated NMR structure of OspE (without the loops) with an *R*-factor of 0.3. After successive rounds of building with Coot (47) and refinement with REFMAC (48) or PHENIX (49), we could identify one OspE molecule bound to a single FH19-20. The loops were modeled during real space refinement using "phenix.refine" software without any applied restraints. The final *R*-factors (R_{work}/R_{free}) of the refined complex structure are 19.3/25.5 (%) (shown in Table 2). The last refinement cycles were done using TLS parameters (nine TLS groups). In the Ramachandran plot, 94.0% of the residues in the structure are in the most favored regions. The structure illustrations have been prepared using PyMOL software (version 1.3, Schrödinger, LLC, New York). The interface between FH19-20 and OspE was analyzed using the PISA (50) server.

TABLE 1
NMR data and structure statistics of the OspE structure

NMR distance constraints	
Distance constraints	
Total	3,446
Intraresidue	736
Interresidue	2,710
Sequential ($\|i-j\|=1$)	809
Medium range ($\|i-j\|<4$)	479
Long range ($\|i-j\|\geq 5$)	1,422
Structure statistics	
Violations (mean and S.D.)	
Distance constraints (Å)	0.0012 ± 0.0001
Maximum distance constraint violation (Å)	0.22 ± 0.04
Deviations from idealized geometry	
Bond lengths (Å)	0.0097 ± 0.0001
Bond angles (degrees)	1.857 ± 0.016
Impropers (degrees)	0.623 ± 0.016
Average pairwise r.m.s.d.[a] (Å)	
Heavy	0.73 ± 0.06
Backbone	0.38 ± 0.05

[a] Pairwise r.m.s.d. was calculated among 20 refined structures of residues 42–171.

Sequence Alignments—Sequence alignments were done using the ClustalW software (51) for Fig. 4 and DALI software (52) for supplemental Fig. 5.

Statistical Analyses—Values are expressed as means ± S.D. All statistical analyses were performed using GraphPad Prism version 5.0.

RESULTS

OspE Consists of an Unexpected Globular Domain with a Flexible N Terminus—The solution structure of OspE was solved by NMR spectroscopy (Table 1 and Fig. 1*a*). Residues 42–171 of OspE form a globular single-domain protein with a backbone root mean square deviation (r.m.s.d.) of 0.38 ± 0.05 Å indicating a well defined structure. OspE has a rigid *a* + *b* fold of eight β-strands and two short α-helices arranged in a repeating topology of four β-strands followed by an α-helix (β1-β2-β3-β4-αI-β5-β6-β7-β8-αII). The β-strands form antiparallel β-sheets, where β1–β4 and β5–β8 are orientated almost perpendicularly. β1 and β8 are held together by hydrogen bonds,

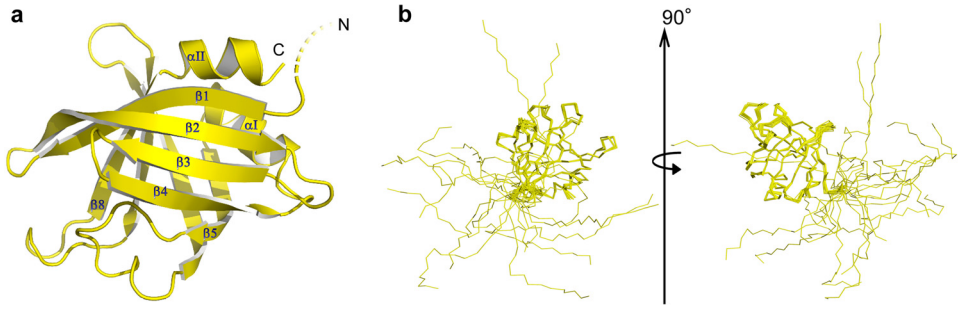

FIGURE 1. **The NMR structure of OspE.** *a*, schematic representation of the mean NMR structure of OspE (residues 21–171, *dashed line* indicating the flexible N terminus). *b*, overlay of 20 energy-minimized NMR structures of OspE with the backbone of residues 42–171 being superimposed. Two orientations are shown rotated 90° from each other.

thus forming an up-down squashed asymmetric β-barrel. It can be viewed as a β-barrel with two distinctive sides, one uniform and another non-uniform. The β2 and β6 strands are highly twisted and deviate from the formation of classic β-barrel strands. β1, β2, and β6 are very long strands (10, 12, and 11 residues, respectively), and β5 along with β8 are the smallest β-strands (6 residues each).

The N-terminal region (residues 20–41) of OspE is structurally flexible, as shown by superimposition of residues 42–171 from 20 NMR structures (Fig. 1*b*). The ^{15}N relaxation data of OspE (supplemental Fig. 2) also show that these residues are moving freely, because of the low T_1/T_2 and $^{15}N\{^1H\}$-NOEs ratio. OspE is attached to the outer membrane via an N-terminal lipid anchor putatively bound to the N-terminal cysteine at position 20 (53). The anchoring topology of OspE is not known, but we can safely assume that the flexible N terminus allows the protein to move freely about its lipid anchor. To assess the tightness of OspE binding to the membrane, we incubated killed *Borrelia* in a buffer for up to 24 h and after centrifugation analyzed the detached OspE from the supernatant. The amount of OspE in the supernatant was low and did not increase as a function of time (supplemental Fig. 6), indicating tight anchoring of OspE to the bacterial surface.

A DALI (52) search showed that the globular domain of OspE resembles the SsgA-like protein (SALP) family of proteins (54), certain DNA/RNA-binding proteins (55–58), some fatty acid-binding proteins (55, 59, 60), and the "Homer" family of proteins (61, 62) (supplemental Fig. 5). The fold has never, to our knowledge, been reported in any extracellular or immune evasion-related molecule from any microbe. OspE has less than 15% sequence identity to any member of the structural family (supplemental Fig. 5). The mammalian PUR-α protein, which binds nucleic acids, has been reported to be involved in immune evasion of viruses like John Cunningham virus and human immunodeficiency virus (HIV) (58). The nucleic acid binding proteins that were found to be structural relatives of OspE were mainly from the "Whirly" protein group, so named because of the resemblance of their quaternary structure to a whirligig.

The OspE·FH19-20 Complex Reveals the Interacting Surfaces—Optimization of heterodimer formation by gel filtration analysis of OspE and FH19-20 (Fig. 2*a*) enabled us to crystallize OspE in complex with FH19-20 (supplemental Fig. 1*b*). Using the optimized 1:1 molar ratio of the proteins, we obtained rod-shaped co-crystals of OspE and FH19-20 in the presence of 2 M ammonium sulfate, 0.1 M citric acid, and 0.2 M sodium chloride (pH 5.5) at 20 °C. The crystal structure of the OspE·FH19-20 complex was solved at 2.83 Å resolution (Table 2 and Fig. 2*b*) using our previously solved FH19-20 structure (35) and the NMR structure of OspE (described above) as models in molecular replacement (Fig. 2*b*). In the complex, OspE binds to domain 20 of FH with a contact surface area of 691 Å. The complex is held together by an $E68_{OspE}$-$R1182_{FH}$-$D73_{OspE}$ ion triple, which is also buttressed by a sulfate group forming an $Arg^{1182}{}_{FH}$-SO_4^{2-}-$Arg^{66}{}_{OspE}$ ion triple, whereas $Arg^{1182}{}_{FH}$ also forms an ion pair with $Glu^{1198}{}_{FH}$ (Fig. 2, *c* and *d*). These interactions form the top part of a pocket for $Trp^{1183}{}_{FH}$, which makes hydrophobic contacts with the aliphatic side chain of $Arg^{1182}{}_{FH}$ and with the OspE backbone around Gly^{75} and Ala^{83} (Table 3).

The OspE structures in solution (NMR) and in complex with FH19-20 (x-ray) were very similar (backbone r.m.s.d. of 1.43 Å/Cα) (supplemental Fig. 7*a*). The structure of FH19-20 in complex with OspE was also practically identical to the published structures of FH19-20 in homotetramers (35) (backbone r.m.s.d. 1.43 Å/Cα) or in the FH19-20·C3d complex (20) (backbone r.m.s.d. 1.15 Å/Cα) (supplemental Fig. 7*b*). The sulfate ion found in the OspE·FH19-20 interface did not affect the orientation of the side chain of FH R1182 (supplemental Fig. 8, *a* and *b*). When the region of OspE close to the sulfate ion was compared between the NMR ensemble and the crystal complex structure, it was observed that orientation of Glu^{68} was similar, whereas that of Arg^{66} was slightly different, most probably due to a hydrogen bond between the NH_2 of Arg^{66} and the oxygen of Arg^{1182} (shown in *red* in supplemental Fig. 8*a*).

The Interaction Site on OspE Confirmed by NMR Analysis—To verify the observed interface between OspE and FH19-20, we analyzed chemical shift perturbations in the NMR spectrum of OspE upon the addition of saturating concentrations of wild type FH19-20 (Fig. 3*a* and supplemental Fig. 3). The residues of OspE that shifted most (>0.4 ppm) are clustered on β-strands 1–4, which form the core of the OspE·FH19-20 interface in the crystal structure (Fig. 3*b*). Of the nine OspE residues involved in hydrogen bonding, six could be assigned in the assay, and five of those were among the residues that shifted most (>0.4 ppm) (Table 3). The other three residues involved in binding (Arg^{66}, Gly^{80}, and Thr^{84}) could not be assigned in the spectra of the FH19-20-bound OspE, probably due to large changes in the

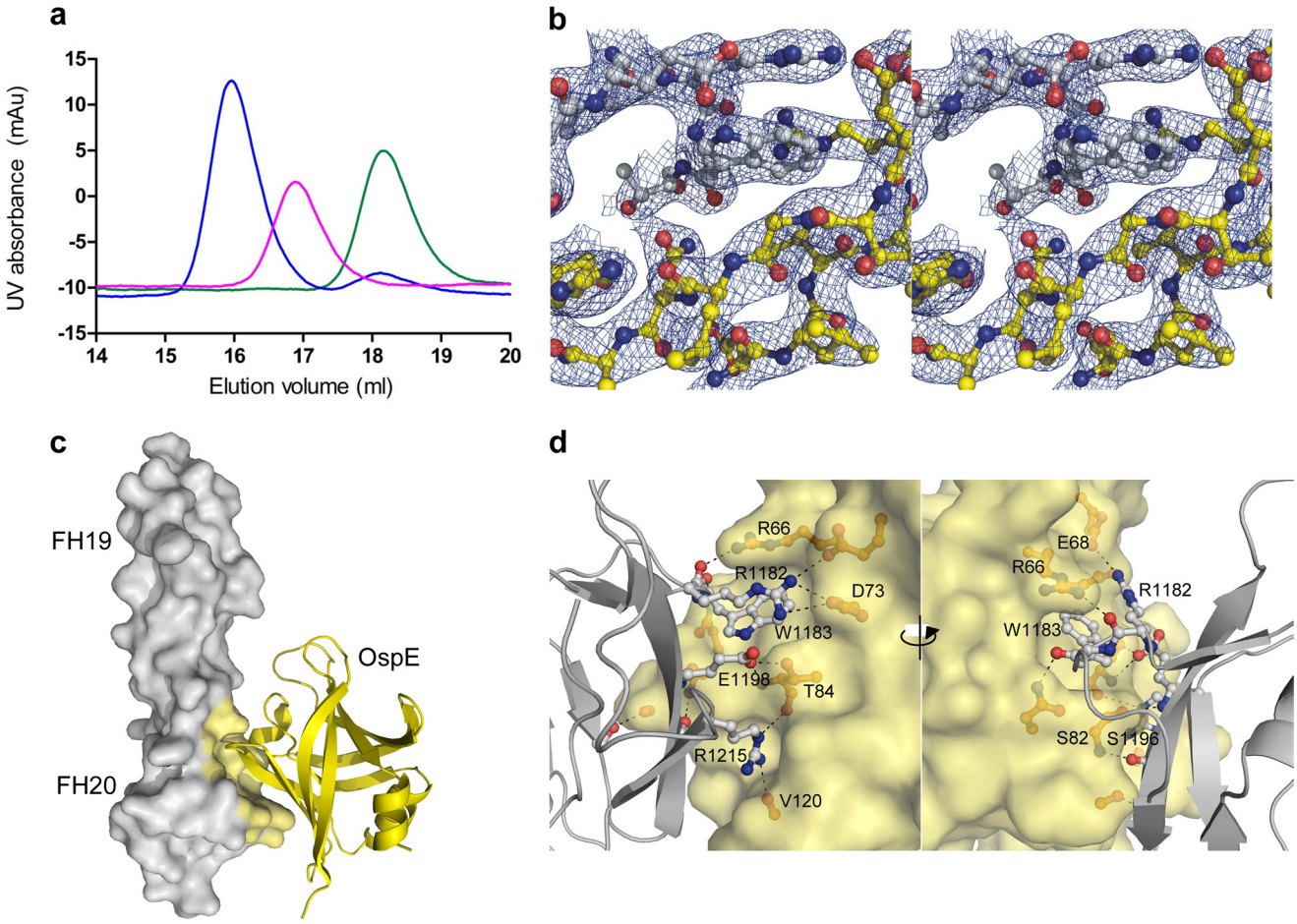

FIGURE 2. **OspE·FH19-20 complex formation and the x-ray crystal structure.** *a*, gel filtration analysis of OspE (*magenta*), FH19-20 (*green*), and OspE·FH19-20 complex (*blue*). *b*, a detail of the electron density map ($2F_O - F_C$) of the OspE·FH19-20 complex in *stereo*. Carbon atoms of FH19-20 are shown in *gray*, and those of OspE are shown in *yellow*. *c*, crystal structure of OspE (*yellow schematic*) in complex with FH19-20 (*gray surface model*, interacting atoms in *yellow*). *d*, interface between FH domain 20 (*gray schematic*) and OspE (*yellow surface model*) from two directions about 180° apart with the interacting residues shown in a *ball-and-stick representation* and the main interacting residues annotated.

TABLE 2

Crystallographic data and refinement of the OspE·FH19-20 complex structure

Data collection	
Space group	$P3_121$
Cell dimensions	
a, b, *c* (Å)	86.4, 86.4, 107.8
α, β, γ (degrees)	90, 90, 120
R_{merge}	17.0 (109.8)[a]
$I/\delta I$	9.99 (2.45)
Completeness (%)	99.2 (100)
Redundancy	7.05 (7.08)
Refinement	
Resolution range (Å)	19.5–2.83 (2.93–2.83)
No. of reflections (unique/observed)	11,501/8,0778
R_{work}/ R_{free} (%)	19.3/25.5
No. of atoms	
Protein	1,913
Ligand/SO_4	5
Water	15
B-factors	
Protein	64.6
Ligand/ion	58.8
Water	49.2
r.m.s.d.	
Bond lengths (Å)	0.012
Bond angles (degrees)	1.37

[a] Data of the highest resolution shell is shown in parentheses.

microenvironment caused by formation of the complex. We confirmed the interface of OspE from the FH19-20 side using mutants of FH19-20 that we have reported elsewhere (34).

The OspE Binding Site Overlaps with the Heparin and Endothelial Cell Binding Sites on FH—The OspE binding site was next compared with the previously mapped binding sites for heparin or endothelial cells on FH domain 20 (Fig. 3*c*). Mutations in residues Arg^{1182}, Lys^{1186}, Lys^{1188}, Arg^{1203}, Arg^{1206}, Arg^{1210}, Arg^{1215}, and Lys^{1230} impair binding of FH19-20 to heparin (37, 63, 64). Of these eight residues, five are on the same side of FH19-20 as the binding site for OspE, and two (Arg^{1182} and Arg^{1215}) directly interact with OspE. This indicates that the heparin/endothelial cell binding site and the OspE binding site on FH domain 20 overlap.

The OspE Residues Mediating Binding to FH19-20 Are Conserved—The sequence identity between OspE and the other FH-binding Erp paralog proteins (*i.e.* the OspE or BbCRASP-3 protein family) is more than 85% (Fig. 4). The sequence alignment shows that, considering only the subset of Erp paralog proteins from *B. burgdorferi* sensu stricto that bind FH, eight of the nine OspE residues that form hydrogen bonds with FH19-20 in the crystal structure are conserved. Arg^{66}, Glu^{68}, Asn^{77}, Gly^{80}, Thr^{84}, and Tyr^{114} are identical in all of the FH-binding Erp paralog proteins (Fig. 4), and Asp^{73} and Ser^{82} were conserved, being replaced by the conservative D73E and S82T mutations in some of the proteins. Seven of

TABLE 3

Hydrogen bonds at the OspE·FH19-20 interface in the crystal structure along with the chemical shift perturbations of the concerned residues

FH19-20 residue (atom)	Distance	OspE residue (atom)	Chemical shift perturbation in $^{1}H,^{15}N$ HSQC spectra
	Å		*ppm*
Arg^{1182} (NH)	3.50	Asp^{73} (OD2)	0.71
Arg^{1182} (NH_2)	2.93	Asp^{73} (OD2)	0.71
Arg^{1182} (NH_2)	3.25	Glu^{68} (OE1)	0.13
Arg^{1182} (O)	2.91	Arg^{66} (NH2)	—[a]
Trp^{1183} (O)	2.96	Asn^{77} (ND2)	0.72
Ser^{1191} (OG)	2.69	Gly^{80} (O)	—
Glu^{1195} (OE2)	3.50	Tyr^{114} (OH)	0.58
Ser^{1196} (O)	2.89	Ser^{82} (N)	1.01
Glu^{1198} (N)	2.93	Ser^{82} (O)	1.01
Glu^{1198} (OE1)	2.89	Thr^{84} (N)	—
Glu^{1198} (OE1)	2.51	Thr^{84} (OG1)	—
Arg^{1215} (NH_2)	2.72	Val^{120} (O)	0.20

[a] —, atoms with larger than 0.4-ppm perturbation were considered to be significantly perturbed upon interaction of OspE with FH19-20.

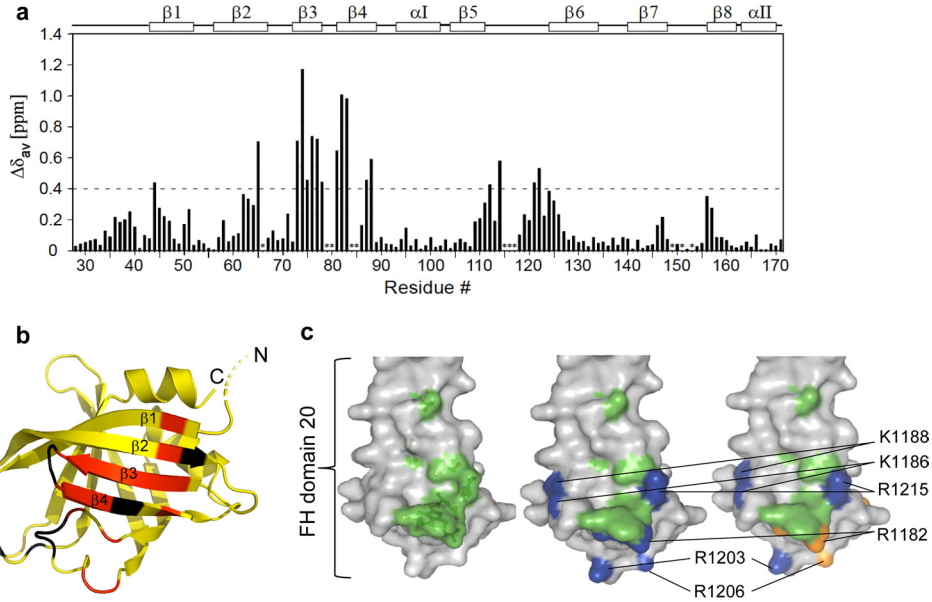

FIGURE 3. **The interaction site between OspE and FH19-20.** *a*, chemical shift perturbation of OspE residues in an HSQC titration NMR experiment upon the addition of FH19-20 (residues not assigned indicated with *asterisks*). *b*, residues with larger that 0.4 ppm (*dotted line*) perturbation considered to interact with FH19-20 are *colored red* in the schematic representation of OspE, whereas residues not observed in the OspE-FH19-20 complex are *colored black*. The β-strands involved are indicated (β1–β4). *c*, surface representation of FH domain 20 with the OspE-binding residues found in the crystal structure *highlighted* in *green* (*left*), the heparin-binding residues highlighted in *blue* (*middle*), and the endothelial cell-binding residues highlighted in *orange* (*right*). The key heparin and endothelial cell binding residues have been annotated.

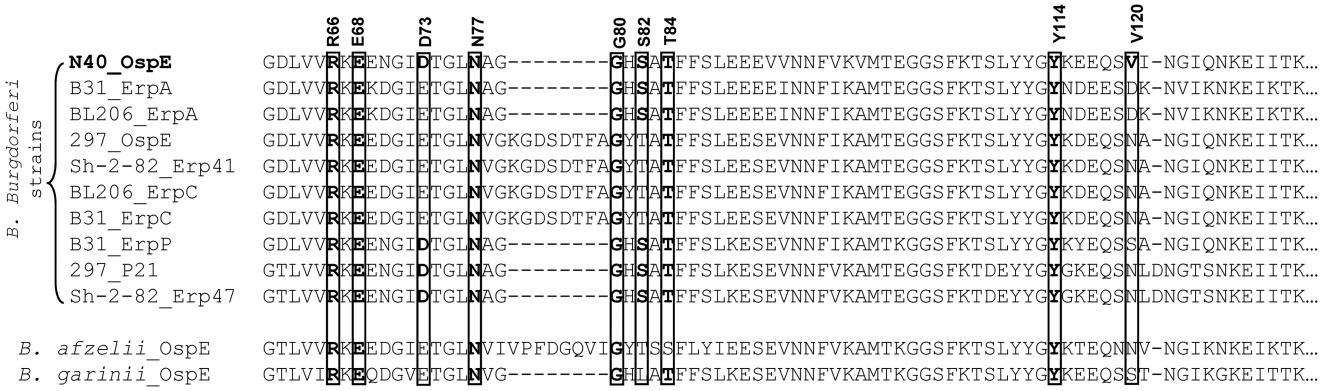

FIGURE 4. **Sequence alignment of the FH binding region of OspE with the homologous parts of the Erps.** Sequence alignment between OspE from the N40 strain of *B. burgdorferi* (used in this study) and Erp paralog proteins encoded by other FH-binding *B. burgdorferi* strains (B31, BL206, 297, and Sh-2-82) and single strains of *B. afzelii* and *B. garinii* is shown. Residues of OspE forming hydrogen bonds with FH19-20 are annotated, their alignments are shown with *boxes*, and identical residues are highlighted in *boldface type*.

the nine residues were also conserved in the OspEs from *B. afzelii* and *B. garinii* (all except for Ser^{82} and Val^{120}) (Fig. 4).

The OspE Binding Site Is Available in FH19-20 Bound to C3b—To analyze if the OspE binding site is available on FH19-20 bound to its physiological ligand C3b, we superim-

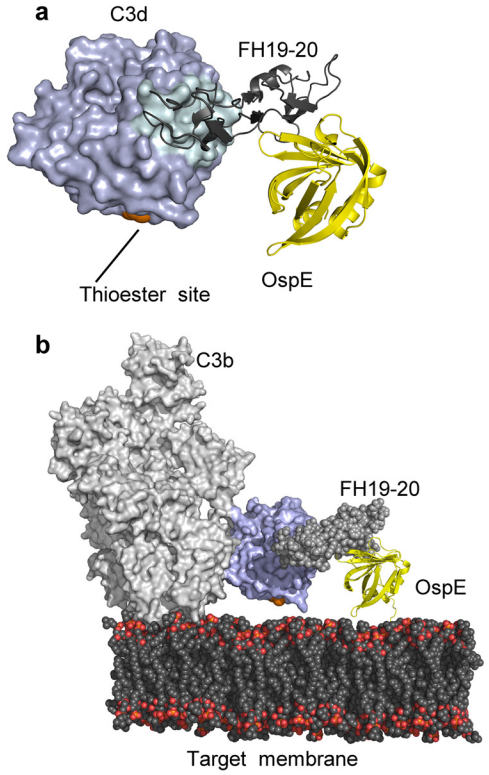

FIGURE 5. **Superimposition based models of OspE in complex with FH19-20 and C3d or C3b.** *a*, superimposition of the OspE·FH19-20 structure with the FH19-20·C3d structure (20), indicating no steric clashes in the OspE·FH19-20·C3d complex. *b*, model of the spatial organization of the OspE·FH19-20 complex bound to C3b (65) on the target surface as based on superimposition of the OspE·FH19-20·C3d complex model with the structure of C3b (containing the C3d domain). The location of the thioester site is indicated in *orange*.

posed our OspE·FH19-20 complex structure on the previously solved structure of FH19-20 in complex with C3d (20) by superimposing FH19-20 structures. The r.m.s.d. of Cα for the superimposed FH19-20 structures was only 0.9 Å, and there were no steric clashes between OspE and C3d. Next we generated an OspE·FH19-20·C3b complex by superimposing the C3d from our OspE·FH19-20·C3d superimposition model on the structure of C3b (containing the C3d domain, also called the thioester domain) (65). In this model, OspE had no steric clashes with any part of C3b, and most importantly, OspE and the thioester site of C3b faced the same direction without blocking each other (Fig. 5*b*). This indicates that FH bound to OspE on the borrelial surface is sterically able to bind a C3b molecule deposited onto the same surface. This is consistent with the role of OspE in mediating complement evasion of *B. burgdorferi*.

DISCUSSION

This study resolves the underlying molecular mechanism of complement evasion by *B. burgdorferi*. It reveals the structural fold of borrelial OspE, identifies the binding surfaces and residues used for the interaction between OspE and host FH, shows the similarity in binding of FH19-20 to the host endothelial cell surface via the heparin binding site and to the microbial OspE protein, and finally explains how FH recruited by OspE onto the borrelial surface is sterically able to eliminate the central complement component C3b on the same surface.

A previous computational analysis suggested that the structure of OspE was composed of coiled coil motifs (66). Our structure, however, clearly shows that this is wrong; OspE has an eight-stranded up-down β-barrel globular structure (residues 42–171) linked to the membrane by a very flexible 21-amino acid tail (Fig. 1*b*). A DALI (52) search indicated that the structural fold has been found in a trimeric protein from the SALP family, several proteins from the "nucleic acid-binding protein" group, some proteins from the "fatty acid-binding protein" family, and a few proteins from the Homer family (supplemental Fig. 5). The sequence homology between OspE and its structural relative proteins is less than 15%, explaining why the structural similarity has not been identified earlier. As far as we know, this is the first time this fold has been identified in any extracellular or immune evasion-related protein of microbial origin. Of the OspE distant homologues, the mammalian transcriptional activator PUR-α appears to be involved in viral immune evasion (58) by acting as the host factor for viral replication. Distant structural homologues of OspE are also found among the Homer family of proteins. Certain members of this family are involved in neuronal plasticity by binding to and regulating metabotropic glutamate receptors (67), whereas others function by binding to members of the nuclear factor of activated T cells (NFAT) family of proteins and down-regulating T-cell activation (62). There is, however, no similarity in the ligand-binding residues between PUR-α or Homer proteins and OspE, which is hardly surprising given the difference in the charge properties of the two ligands. The fatty acid-binding proteins that have a β-sheet structure similar to that of OspE mainly interact with the fatty acids via the residues inside the hydrophobic core of the protein (55, 59, 60).

The fold of the globular domain seems to be stable and fairly rigid because the r.m.s.d. of the globular domain of the 20 NMR structures was only 0.38 $\pm$ 0.05 Å for the backbone atoms, and the structures of the liganded (x-ray) and unliganded (NMR) OspE were very similar (r.m.s.d. of 1.43 Å for Cα atoms) (supplemental Fig. 7*a*). The length of the extended, structurally flexible tail is more than 50 Å. Although the anchor topology of OspE is not known, trypsinolysis studies on the anchor topologies of borrelial OspA and Vsp1 proteins indicate that in both OspA (N-terminal tethering domain of just 12 residues) and Vsp1 (tethering domain of 21 residues), the tail is on the outside. In OspA, residues in positions 6–11 can be cleaved by trypsin, whereas in Vsp1, residues in positions 7–14 can be cleaved (68, 69); *i.e.* most of the N-terminal tail in both proteins is surface-exposed and thus cannot be part of a protein membrane anchor but is instead presumably part of a flexible linker. Consequently, the most plausible anchoring topology for OspE is that it binds through a triacyl cysteine anchor, and the N-terminal region provides flexibility. Our results on incubation of killed *Borrelia* (supplemental Fig. 6) indicate that the majority of OspE is tightly bound to the borrelial surface and suggests that it is bound very firmly to the OM, indeed. Such a lipid anchor would provide OspE with good lateral mobility in the membrane, whereas the longer tethering domain would allows OspE the freedom to rotate and tilt. OspE can obviously bind to host FH on the cell surface because the binding site is far from the tethering domains.

In our OspE·FH19-20 structure, four residues (Arg^{1182}, Trp^{1183}, Glu^{1198}, and Arg^{1215}) in the FH C terminus play a key role in binding to OspE. The central role of these residues is supported by the chemical shift perturbations in the NMR spectrum of OspE upon the addition of saturating concentrations of wild type FH19-20 (Fig. 3*a* and supplemental Fig. 3) and by a competition binding assay with 14 mutant FH19-20 proteins (34). We have previously proposed, on the basis of alanine scanning mutations to OspE peptides, that multiple lysines in OspE might be required to bind FH19-20 (27). None of the peptides used in that work, however, could inhibit OspE binding to FH19-20 (27), indicating that binding of the linear OspE peptides to FH19-20 was weak. In our OspE·FH19-20 structure, there are no OspE lysines in the interface, so our previous results with peptides did not reflect the true OspE·FH19-20 interaction but an artificial binding of positively charged short linear synthetic peptides to a negatively charged patch on FH19-20.

A sulfate ion was found in the OspE·FH19-20 interface (supplemental Fig. 8*a*). In principle, a sulfate ion could potentially influence orientation of side chains in its vicinity either by steric hindrance or by forming hydrogen bonds. Superposition of the OspE·FH19-20 complex structure with the OspE NMR structure and the WT FH19-20 structure separately (supplemental Fig. 8, *b* and *c*) showed hardly any difference in the side chains close to the sulfate ion. Therefore, the sulfate ion itself obviously has not disturbed the arrangement of the residues within the interface.

Is it possible that the OspE·FH19-20 structure we see is a crystallographic artifact? The NMR-based perturbation assay clearly excludes that possibility because the chemical shift of the OspE residues that interact with FH19-20 in the crystal structure changed when wild type FH19-20 was bound to OspE in solution (Fig. 3*a*). Radioligand binding assays using 14 point-mutated FH19-20 proteins also support our results. Single point mutations of five (R1182A, W1183L, L1189R, E1198A, and R1215Q) of seven key residues in the OspE·FH19-20 interface caused clear impairment in binding of FH19-20 to OspE (34) (the other two were not in the mutation panel). Deletion of the C-terminal 15 residues of the highly homologous OspE paralog p21 impairs, but does not abolish, binding to FH, whereas deletion of the N-terminal 35 residues has no effect (27). On the basis of the OspE·FH19-20 structure, it is possible that the effect of the C-terminal OspE deletion is either due to disturbance of the globular OspE fold, because the last 15 residues in OspE form α-helix 2 and part of β-sheet 8, or due to a local effect of the disruption of the β-sheet 8 on the loop between β-sheets 3 and 4 and thereby on the FH-binding residues on those sheets. On the basis of the structure (only part of the β-sheet 8 needed for the barrel was missing) and because the deletion did not abolish binding to FH19-20, it is likely that the deletion did not disrupt the fold completely. Our results thus explain well the previous data with deletion mutants of an OspE homolog.

We and others have earlier shown that binding of FH is essential for *B. burgdorferi* to survive in human serum and that OspE (*i.e.* BbCRASP-3) and BbCRASP-1 (70) are needed for this survival (8, 9, 13, 15, 27). It is obvious that the microbe benefits from the recruitment of host FH onto the microbial surface because FH acts as a cofactor for factor I in the degradation process of the central complement component C3b needed for both opsonization and propagation of the complement cascade to form membrane attack complexes (71). Therefore, it is easy to understand that acquisition of host FH onto *Borrelia* correlates strictly with survival of the spirochetes in non-immune serum or blood.

The C-terminal domains 19 and 20 of FH are known to mediate physiologically important binding of FH to both the C3d part of C3b (19, 20) and heparin/endothelial cells (37, 63, 64). Comparing the binding site of OspE to the previously reported binding sites for these physiological ligands showed that the OspE site overlaps with the heparin/endothelial cell binding site (residues Arg^{1182} and Arg^{1215} and the surrounding region) (37, 63, 64), whereas the C3d/C3b binding site on domain 19 is clearly distinct. This is also clear in the superimposition of the OspE·FH19-20 structure with the previously published FH19-20·C3d structure (20) (Fig. 5*a*). The overlap of the OspE and heparin binding sites indicates that *B. burgdorferi* mimics host cells in acquiring FH with OspE by binding to the same site as host cells bind with heparin. This resembles acquisition of FH by *N. meningitidis* via a heparin binding site on domain 7 of FH (32).

Two requirements have been suggested for physiologically relevant interaction between a microbe and host FH; the microbial binding site on FH needs to be easily accessible, and the cofactor site on FH domains 1–4 must not be disturbed (72). Our work shows that the interaction between FH and OspE fulfills both of these requirements at the structural level, because binding of OspE to FH19-20 does not block binding of FH (neither domains 1–4 nor 19–20) to C3b (20, 73), and the OspE site is fully accessible on FH, as seen in our OspE·FH19-20·C3b model (Fig. 5). Finally, this superimposition shows that the borrelial binding site on FH is directed toward the surface to which C3b is bound to via the thioester bond. This suggests that FH bound to OspE on the borrelial surface can recruit factor I not only to fluid phase C3b but also to opsonizing C3b bound to the borrelial surface, thus preventing both opsonophagocytosis and propagation of the complement cascade to form lytic membrane attack complexes.

Humoral immune response against an outer surface lipoprotein of *B. burgdorferi*, OspA, has been shown to protect humans from Lyme borreliosis (74). Although the OspA-based vaccine against the disease failed due to side effects (75), it indicated that a humoral immune response can protect from Lyme borreliosis. The FH-binding protein from *N. meningitidis* serotype B has recently been successfully used as a candidate for vaccine development against meningococcal disease and is now in phase III clinical trials (76). Therefore, studies aimed at identifying a new borrelial surface antigen, preferably one binding FH, are warranted. A suitable vaccine candidate must 1) be surface-exposed, 2) be conserved among different strains and genospecies of the pathogen, 3) be produced during human infection, 4) be necessary for development of a clinical infection, and 5) raise an immune response in humans *in vivo*. There is an increasing body of evidence that the FH-binding protein OspE meets all of these criteria (13). Our current study

increases the acceptability of OspE as a vaccine candidate because it shows that the residues needed for the OspE·FH19-20 interaction are highly conserved among the different *Borrelia* genospecies and strains (Fig. 4).

Our OspE·FH19-20 structure is the first structure of a microbial protein binding to domains 19 and 20 of FH. It is known that more than 10 pathogenic microbes other than *Borrelia* acquire host FH using the same domains. We have studied the binding of several other microbes to FH19-20, and the data indicate a conserved pattern of microbial acquisition of FH via these domains (34). Domains 19 and 20 of FH are evidently essential for recognition of host cells and surfaces by FH because mutations in these domains lead to a life-threatening disease, atypical hemolytic-uremic syndrome. Therefore, it is logical that microbes use these domains as a key way of avoiding complement attack, and in this report, we have shown an example of how an important and emerging human pathogen, Lyme disease-causing *B. burgdorferi*, utilizes these domains.

Acknowledgments—We thank Miia Eholuoto and Ilkka J. T. Seppälä (University of Helsinki and Huslab, Helsinki University Central Hospital Laboratory) for providing the OspE clone. We acknowledge Marjatta Ahonen, Pirkko Kokkonen, and Kirsti Widing for excellent technical assistance. We also thank ESRF for beamtime on ID14-4, Seija Mäki, Serranda Gashi, and the Biocenter Finland crystallization facility. A. B thanks Prof. Mikael Skurnik for very fruitful scientific discussions.

REFERENCES

1. Barbour, A. G., Maupin, G. O., Teltow, G. J., Carter, C. J., and Piesman, J. (1996) Identification of an uncultivable *Borrelia* species in the hard tick *Amblyomma americanum*. Possible agent of a Lyme disease-like illness. *J. Infect. Dis.* **173,** 403–409
2. Centers for Disease Control and Prevention (CDC) (1996) Lyme disease. United States, 1995. *MMWR Morb. Mortal. Wkly. Rep.* **45,** 481–484
3. Barbour, A. G., and Fish, D. (1993) The biological and social phenomenon of Lyme disease. *Science* **260,** 1610–1616
4. Steere, A. C., Grodzicki, R. L., Kornblatt, A. N., Craft, J. E., Barbour, A. G., Burgdorfer, W., Schmid, G. P., Johnson, E., and Malawista, S. E. (1983) The spirochetal etiology of Lyme disease. *N. Engl. J. Med.* **308,** 733–740
5. Ohnishi, J., Piesman, J., and de Silva, A. M. (2001) Antigenic and genetic heterogeneity of *Borrelia burgdorferi* populations transmitted by ticks. *Proc. Natl. Acad. Sci. U.S.A.* **98,** 670–675
6. Steere, A. C., Malawista, S. E., Hardin, J. A., Ruddy, S., Askenase, W., and Andiman, W. A. (1977) Erythema chronicum migrans and Lyme arthritis. The enlarging clinical spectrum. *Ann. Intern. Med.* **86,** 685–698
7. van Dam, A. P., Kuiper, H., Vos, K., Widjojokusumo, A., de Jongh, B. M., Spanjaard, L., Ramselaar, A. C., Kramer, M. D., and Dankert, J. (1993) Different genospecies of *Borrelia burgdorferi* are associated with distinct clinical manifestations of Lyme borreliosis. *Clin. Infect. Dis.* **17,** 708–717
8. Alitalo, A., Meri, T., Comstedt, P., Jeffery, L., Tornberg, J., Strandin, T., Lankinen, H., Bergström, S., Cinco, M., Vuppala, S. R., Akins, D. R., and Meri, S. (2005) Expression of complement factor H binding immunoevasion proteins in *Borrelia garinii* isolated from patients with neuroborreliosis. *Eur. J. Immunol.* **35,** 3043–3053
9. Alitalo, A., Meri, T., Rämö, L., Jokiranta, T. S., Heikkilä, T., Seppälä, I. J., Oksi, J., Viljanen, M., and Meri, S. (2001) Complement evasion by *Borrelia burgdorferi*. Serum-resistant strains promote C3b inactivation. *Infect. Immun.* **69,** 3685–3691
10. Walport, M. J. (2001) Complement. First of two parts. *N. Engl. J. Med.* **344,** 1058–1066
11. Hartmann, K., Corvey, C., Skerka, C., Kirschfink, M., Karas, M., Brade, V., Miller, J. C., Stevenson, B., Wallich, R., Zipfel, P. F., and Kraiczy, P. (2006) Functional characterization of BbCRASP-2, a distinct outer membrane protein of *Borrelia burgdorferi* that binds host complement regulators factor H and FHL-1. *Mol. Microbiol.* **61,** 1220–1236
12. Kraiczy, P., Hellwage, J., Skerka, C., Becker, H., Kirschfink, M., Simon, M. M., Brade, V., Zipfel, P. F., and Wallich, R. (2004) Complement resistance of *Borrelia burgdorferi* correlates with the expression of BbCRASP-1, a novel linear plasmid-encoded surface protein that interacts with human factor H and FHL-1 and is unrelated to Erp proteins. *J. Biol. Chem.* **279,** 2421–2429
13. Hellwage, J., Meri, T., Heikkilä, T., Alitalo, A., Panelius, J., Lahdenne, P., Seppälä, I. J., and Meri, S. (2001) The complement regulator factor H binds to the surface protein OspE of *Borrelia burgdorferi*. *J. Biol. Chem.* **276,** 8427–8435
14. Hefty, P. S., Jolliff, S. E., Caimano, M. J., Wikel, S. K., Radolf, J. D., and Akins, D. R. (2001) Regulation of OspE-related, OspF-related, and Elp lipoproteins of *Borrelia burgdorferi* strain 297 by mammalian host-specific signals. *Infect. Immun.* **69,** 3618–3627
15. Alitalo, A., Meri, T., Lankinen, H., Seppälä, I., Lahdenne, P., Hefty, P. S., Akins, D., and Meri, S. (2002) Complement inhibitor factor H binding to Lyme disease spirochetes is mediated by inducible expression of multiple plasmid-encoded outer surface protein E paralogs. *J. Immunol.* **169,** 3847–3853
16. de Córdoba, S. R., and de Jorge, E. G. (2008) Translational mini-review series on complement factor H. Genetics and disease associations of human complement factor H. *Clin. Exp. Immunol.* **151,** 1–13
17. Atkinson, J. P., and Goodship, T. H. (2007) Complement factor H and the hemolytic uremic syndrome. *J. Exp. Med.* **204,** 1245–1248
18. Gordon, D. L., Kaufman, R. M., Blackmore, T. K., Kwong, J., and Lublin, D. M. (1995) Identification of complement regulatory domains in human factor H. *J. Immunol.* **155,** 348–356
19. Morgan, H. P., Schmidt, C. Q., Guariento, M., Blaum, B. S., Gillespie, D., Herbert, A. P., Kavanagh, D., Mertens, H. D., Svergun, D. I., Johansson, C. M., Uhrín, D., Barlow, P. N., and Hannan, J. P. (2011) Structural basis for engagement by complement factor H of C3b on a self surface. *Nat. Struct. Mol. Biol.* **18,** 463–470
20. Kajander, T., Lehtinen, M. J., Hyvärinen, S., Bhattacharjee, A., Leung, E., Isenman, D. E., Meri, S., Goldman, A., and Jokiranta, T. S. (2011) Dual interaction of factor H with C3d and glycosaminoglycans in host-nonhost discrimination by complement. *Proc. Natl. Acad. Sci. U.S.A.* **108,** 2897–2902
21. Haapasalo, K., Vuopio, J., Syrjänen, J., Suvilehto, J., Massinen, S., Karppelin, M., Järvelä, I., Meri, S., Kere, J., and Jokiranta, T. S. (2012) Acquisition of complement factor H is important for pathogenesis of *Streptococcus pyogenes* infections. Evidence from bacterial *in vitro* survival and human genetic association. *J. Immunol.* **188,** 426–435
22. Zipfel, P. F., Hallström, T., Hammerschmidt, S., and Skerka, C. (2008) The complement fitness factor H. Role in human diseases and for immune escape of pathogens, like pneumococci. *Vaccine* **26,** I67–I74
23. Lambris, J. D., Ricklin, D., and Geisbrecht, B. V. (2008) Complement evasion by human pathogens. *Nat. Rev. Microbiol.* **6,** 132–142
24. Meri, T., Hartmann, A., Lenk, D., Eck, R., Würzner, R., Hellwage, J., Meri, S., and Zipfel, P. F. (2002) The yeast *Candida albicans* binds complement regulators factor H and FHL-1. *Infect. Immun.* **70,** 5185–5192
25. Ho, D. K., Jarva, H., and Meri, S. (2010) Human complement factor H binds to outer membrane protein Rck of *Salmonella*. *J. Immunol.* **185,** 1763–1769
26. Kraiczy, P., Skerka, C., Kirschfink, M., Brade, V., and Zipfel, P. F. (2001) Immune evasion of *Borrelia burgdorferi* by acquisition of human complement regulators FHL-1/reconectin and Factor H. *Eur. J. Immunol.* **31,** 1674–1684
27. Alitalo, A., Meri, T., Chen, T., Lankinen, H., Cheng, Z. Z., Jokiranta, T. S., Seppälä, I. J., Lahdenne, P., Hefty, P. S., Akins, D. R., and Meri, S. (2004) Lysine-dependent multipoint binding of the *Borrelia burgdorferi* virulence factor outer surface protein E to the C terminus of factor H. *J. Immunol.* **172,** 6195–6201
28. Amdahl, H., Jarva, H., Haanperä, M., Mertsola, J., He, Q., Jokiranta, T. S., and Meri, S. (2011) Interactions between *Bordetella pertussis* and the complement inhibitor factor H. *Mol. Immunol.* **48,** 697–705

29. McDowell, J. V., Harlin, M. E., Rogers, E. A., and Marconi, R. T. (2005) Putative coiled-coil structural elements of the BBA68 protein of Lyme disease spirochetes are required for formation of its factor H binding site. *J. Bacteriol.* **187,** 1317–1323
30. Blackmore, T. K., Hellwage, J., Sadlon, T. A., Higgs, N., Zipfel, P. F., Ward, H. M., and Gordon, D. L. (1998) Identification of the second heparin-binding domain in human complement factor H. *J. Immunol.* **160,** 3342–3348
31. Blackmore, T. K., Sadlon, T. A., Ward, H. M., Lublin, D. M., and Gordon, D. L. (1996) Identification of a heparin binding domain in the seventh short consensus repeat of complement factor H. *J. Immunol.* **157,** 5422–5427
32. Schneider, M. C., Prosser, B. E., Caesar, J. J., Kugelberg, E., Li, S., Zhang, Q., Quoraishi, S., Lovett, J. E., Deane, J. E., Sim, R. B., Roversi, P., Johnson, S., Tang, C. M., and Lea, S. M. (2009) *Neisseria meningitidis* recruits factor H using protein mimicry of host carbohydrates. *Nature* **458,** 890–893
33. Batsford, S., Rust, C., and Neubert, U. (1998) Analysis of antibody response to the outer surface protein family in lyme borreliosis patients. *J. Infect. Dis.* **178,** 1676–1683
34. Meri, T., Amdahl, H., Lehtinen, M. J., Hyvärinen, S., McDowell, J. V., Bhattacharjee, A., Meri, S., Marconi, R., Goldman, A., and Jokiranta, T. S. (2013) Microbes bind complement inhibitor factor H via a common site. *PLoS Pathog.* **9,** e1003308
35. Jokiranta, T. S., Jaakola, V. P., Lehtinen, M. J., Pärepalo, M., Meri, S., and Goldman, A. (2006) Structure of complement factor H carboxyl-terminus reveals molecular basis of atypical haemolytic uremic syndrome. *EMBO J.* **25,** 1784–1794
36. Bhattacharjee, A., Lehtinen, M. J., Kajander, T., Goldman, A., and Jokiranta, T. S. (2010) Both domain 19 and domain 20 of factor H are involved in binding to complement C3b and C3d. *Mol. Immunol.* **47,** 1686–1691
37. Lehtinen, M. J., Rops, A. L., Isenman, D. E., van der Vlag, J., and Jokiranta, T. S. (2009) Mutations of factor H impair regulation of surface-bound C3b by three mechanisms in atypical hemolytic uremic syndrome. *J. Biol. Chem.* **284,** 15650–15658
38. Muona, M., Aranko, A. S., and Iwai, H. (2008) Segmental isotopic labelling of a multidomain protein by protein ligation by protein trans-splicing. *Chembiochem* **9,** 2958–2961
39. Delaglio, F., Grzesiek, S., Vuister, G. W., Zhu, G., Pfeifer, J., and Bax, A. (1995) NMRPipe. A multidimensional spectral processing system based on UNIX pipes. *J. Biomol. NMR* **6,** 277–293
40. Vranken, W. F., Boucher, W., Stevens, T. J., Fogh, R. H., Pajon, A., Llinas, M., Ulrich, E. L., Markley, J. L., Ionides, J., and Laue, E. D. (2005) The CCPN data model for NMR spectroscopy. Development of a software pipeline. *Proteins* **59,** 687–696
41. Güntert, P., Mumenthaler, C., and Wüthrich, K. (1997) Torsion angle dynamics for NMR structure calculation with the new program DYANA. *J. Mol. Biol.* **273,** 283–298
42. Herrmann, T., Güntert, P., and Wüthrich, K. (2002) Protein NMR structure determination with automated NOE assignment using the new software CANDID and the torsion angle dynamics algorithm DYANA. *J. Mol. Biol.* **319,** 209–227
43. Laskowski, R. A., Rullmannn, J. A., MacArthur, M. W., Kaptein, R., and Thornton, J. M. (1996) AQUA and PROCHECK-NMR. Programs for checking the quality of protein structures solved by NMR. *J. Biomol. NMR* **8,** 477–486
44. Farrow, N. A., Muhandiram, R., Singer, A. U., Pascal, S. M., Kay, C. M., Gish, G., Shoelson, S. E., Pawson, T., Forman-Kay, J. D., and Kay, L. E. (1994) Backbone dynamics of a free and phosphopeptide-complexed Src homology 2 domain studied by ^{15}N NMR relaxation. *Biochemistry* **33,** 5984–6003
45. Kabsch, W. (2010) XDS. *Acta Crystallogr. D Biol. Crystallogr.* **66,** 125–132
46. DiMaio, F., Tyka, M. D., Baker, M. L., Chiu, W., and Baker, D. (2009) Refinement of protein structures into low resolution density maps using Rosetta. *J. Mol. Biol.* **392,** 181–190
47. Emsley, P., and Cowtan, K. (2004) Coot. Model-building tools for molecular graphics. *Acta Crystallogr. D Biol. Crystallogr.* **60,** 2126–2132
48. Murshudov, G. N., Vagin, A. A., and Dodson, E. J. (1997) Refinement of macromolecular structures by the maximum-likelihood method. *Acta Crystallogr. D Biol. Crystallogr.* **53,** 240–255
49. Adams, P. D., Grosse-Kunstleve, R. W., Hung, L. W., Ioerger, T. R., McCoy, A. J., Moriarty, N. W., Read, R. J., Sacchettini, J. C., Sauter, N. K., and Terwilliger, T. C. (2002) PHENIX. Building new software for automated crystallographic structure determination. *Acta Crystallogr. D Biol. Crystallogr.* **58,** 1948–1954
50. Krissinel, E., and Henrick, K. (2007) Inference of macromolecular assemblies from crystalline state. *J. Mol. Biol.* **372,** 774–797
51. Larkin, M. A., Blackshields, G., Brown, N. P., Chenna, R., McGettigan, P. A., McWilliam, H., Valentin, F., Wallace, I. M., Wilm, A., Lopez, R., Thompson, J. D., Gibson, T. J., and Higgins, D. G. (2007) Clustal W and Clustal X version 2.0. *Bioinformatics* **23,** 2947–2948
52. Holm, L., and Rosenström, P. (2010) Dali server. Conservation mapping in 3D. *Nucleic Acids Res.* **38,** W545–W549
53. Lam, T. T., Nguyen, T. P., Montgomery, R. R., Kantor, F. S., Fikrig, E., and Flavell, R. A. (1994) Outer surface proteins E and F of *Borrelia burgdorferi*, the agent of Lyme disease. *Infect. Immun.* **62,** 290–298
54. Xu, Q., Traag, B. A., Willemse, J., McMullan, D., Miller, M. D., Elsliger, M. A., Abdubek, P., Astakhova, T., Axelrod, H. L., Bakolitsa, C., Carlton, D., Chen, C., Chiu, H. J., Chruszcz, M., Clayton, T., Das, D., Deller, M. C., Duan, L., Ellrott, K., Ernst, D., Farr, C. L., Feuerhelm, J., Grant, J. C., Grzechnik, A., Grzechnik, S. K., Han, G. W., Jaroszewski, L., Jin, K. K., Klock, H. E., Knuth, M. W., Kozbial, P., Krishna, S. S., Kumar, A., Marciano, D., Minor, W., Mommaas, A. M., Morse, A. T., Nigoghossian, E., Nopakun, A., Okach, L., Oommachen, S., Paulsen, J., Puckett, C., Reyes, R., Rife, C. L., Sefcovic, N., Tien, H. J., Trame, C. B., van den Bedem, H., Wang, S., Weekes, D., Hodgson, K. O., Wooley, J., Deacon, A. M., Godzik, A., Lesley, S. A., Wilson, I. A., and van Wezel, G. P. (2009) Structural and functional characterizations of SsgB, a conserved activator of developmental cell division in morphologically complex actinomycetes. *J. Biol. Chem.* **284,** 25268–25279
55. Sharma, A. (2011) Fatty acid induced remodeling within the human liver fatty acid-binding protein. *J. Biol. Chem.* **286,** 31924–31928
56. Schumacher, M. A., Karamooz, E., Ziková, A., Trantírek, L., and Lukes, J. (2006) Crystal structures of *T. brucei* MRP1/MRP2 guide-RNA binding complex reveal RNA matchmaking mechanism. *Cell* **126,** 701–711
57. Desveaux, D., Allard, J., Brisson, N., and Sygusch, J. (2002) A new family of plant transcription factors displays a novel ssDNA-binding surface. *Nat. Struct. Biol.* **9,** 512–517
58. Graebsch, A., Roche, S., and Niessing, D. (2009) X-ray structure of Pur-α reveals a Whirly-like fold and an unusual nucleic-acid binding surface. *Proc. Natl. Acad. Sci. U.S.A.* **106,** 18521–18526
59. Capaldi, S., Guariento, M., Saccomani, G., Fessas, D., Perduca, M., and Monaco, H. L. (2007) A single amino acid mutation in zebrafish (*Danio rerio*) liver bile acid-binding protein can change the stoichiometry of ligand binding. *J. Biol. Chem.* **282,** 31008–31018
60. Nichesola, D., Perduca, M., Capaldi, S., Carrizo, M. E., Righetti, P. G., and Monaco, H. L. (2004) Crystal structure of chicken liver basic fatty acid-binding protein complexed with cholic acid. *Biochemistry* **43,** 14072–14079
61. Beneken, J., Tu, J. C., Xiao, B., Nuriya, M., Yuan, J. P., Worley, P. F., and Leahy, D. J. (2000) Structure of the Homer EVH1 domain-peptide complex reveals a new twist in polyproline recognition. *Neuron* **26,** 143–154
62. Huang, G. N., Huso, D. L., Bouyain, S., Tu, J., McCorkell, K. A., May, M. J., Zhu, Y., Lutz, M., Collins, S., Dehoff, M., Kang, S., Whartenby, K., Powell, J., Leahy, D., and Worley, P. F. (2008) NFAT binding and regulation of T cell activation by the cytoplasmic scaffolding Homer proteins. *Science* **319,** 476–481
63. Herbert, A. P., Deakin, J. A., Schmidt, C. Q., Blaum, B. S., Egan, C., Ferreira, V. P., Pangburn, M. K., Lyon, M., Uhrín, D., and Barlow, P. N. (2007) Structure shows that a glycosaminoglycan and protein recognition site in factor H is perturbed by age-related macular degeneration-linked single nucleotide polymorphism. *J. Biol. Chem.* **282,** 18960–18968
64. Ferreira, V. P., Herbert, A. P., Cortés, C., McKee, K. A., Blaum, B. S., Esswein, S. T., Uhrín, D., Barlow, P. N., Pangburn, M. K., and Kavanagh, D. (2009) The binding of factor H to a complex of physiological polyanions and C3b on cells is impaired in atypical hemolytic uremic syndrome. *J. Immunol.* **182,** 7009–7018

65. Janssen, B. J., Christodoulidou, A., McCarthy, A., Lambris, J. D., and Gros, P. (2006) Structure of C3b reveals conformational changes that underlie complement activity. *Nature* **444,** 213–216
66. McDowell, J. V., Wolfgang, J., Senty, L., Sundy, C. M., Noto, M. J., and Marconi, R. T. (2004) Demonstration of the involvement of outer surface protein E coiled coil structural domains and higher order structural elements in the binding of infection-induced antibody and the complement-regulatory protein, factor H. *J. Immunol.* **173,** 7471–7480
67. Brakeman, P. R., Lanahan, A. A., O'Brien, R., Roche, K., Barnes, C. A., Huganir, R. L., and Worley, P. F. (1997) Homer. A protein that selectively binds metabotropic glutamate receptors. *Nature* **386,** 284–288
68. Chen, S., and Zückert, W. R. (2011) Probing the *Borrelia burgdorferi* surface lipoprotein secretion pathway using a conditionally folding protein domain. *J. Bacteriol.* **193,** 6724–6732
69. Chen, S., Kumru, O. S., and Zückert, W. R. (2011) Determination of *Borrelia* surface lipoprotein anchor topology by surface proteolysis. *J. Bacteriol.* **193,** 6379–6383
70. Cordes, F. S., Roversi, P., Kraiczy, P., Simon, M. M., Brade, V., Jahraus, O., Wallis, R., Skerka, C., Zipfel, P. F., Wallich, R., and Lea, S. M. (2005) A novel fold for the factor H-binding protein BbCRASP-1 of *Borrelia burgdorferi*. *Nat. Struct. Mol. Biol.* **12,** 276–277
71. Pangburn, M. K., and Müller-Eberhard, H. J. (1978) Complement C3 convertase. Cell surface restriction of β1H control and generation of restriction on neuraminidase-treated cells. *Proc. Natl. Acad. Sci. U.S.A.* **75,** 2416–2420
72. Ferreira, V. P., Pangburn, M. K., and Cortés, C. (2010) Complement control protein factor H. The good, the bad, and the inadequate. *Mol. Immunol.* **47,** 2187–2197
73. Wu, J., Wu, Y. Q., Ricklin, D., Janssen, B. J., Lambris, J. D., and Gros, P. (2009) Structure of complement fragment C3b-factor H and implications for host protection by complement regulators. *Nat. Immunol.* **10,** 728–733
74. Fikrig, E., Barthold, S. W., Kantor, F. S., and Flavell, R. A. (1991) Protection of mice from Lyme borreliosis by oral vaccination with *Escherichia coli* expressing OspA. *J. Infect. Dis.* **164,** 1224–1227
75. Rosé, C. D., Fawcett, P. T., and Gibney, K. M. (2001) Arthritis following recombinant outer surface protein A vaccination for Lyme disease. *J. Rheumatol.* **28,** 2555–2557
76. Giuliani, M. M., Adu-Bobie, J., Comanducci, M., Aricò, B., Savino, S., Santini, L., Brunelli, B., Bambini, S., Biolchi, A., Capecchi, B., Cartocci, E., Ciucchi, L., Di Marcello, F., Ferlicca, F., Galli, B., Luzzi, E., Masignani, V., Serruto, D., Veggi, D., Contorni, M., Morandi, M., Bartalesi, A., Cinotti, V., Mannucci, D., Titta, F., Ovidi, E., Welsch, J. A., Granoff, D., Rappuoli, R., and Pizza, M. (2006) A universal vaccine for serogroup B meningococcus. *Proc. Natl. Acad. Sci. U.S.A.* **103,** 10834–10839

Bhattacharjee et al

Structural basis for complement evasion by Lyme disease pathogen *Borrelia burgdorferi*

SUPPLEMENTARY MATERIAL

Supplementary Figure 1. SDS-PAGE, Gel filtration and MALS analysis of OspE and OspE:FH1920 complex respectively

Supplementary Figure 2. The OspE ^{15}N relaxation data.

Supplementary Figure 3. ^{15}N-HSQC spectrum of OspE alone and TROSY ^{15}N-HSQC of OspE saturated with wild type FH19-20.

Supplementary Figure 4. Binding studies of wild type FH19-20 and the TheFH19-20$_{D1119G,Q1139A}$ mutant to OspE.

Supplementary Figure 5. A DALI based alignment (sequence and secondary structure) of the different OspE structural homologues identified by DALI.

Supplementary Figure 6. Release of OspE from *B. burgdorferi* s.s.

Supplementary Figure 7. Structural alignment of the different OspE and FH19-20 structures.

Supplementary Figure 8. Close view of the SO4 ion in the FH19-20:OspE complex.

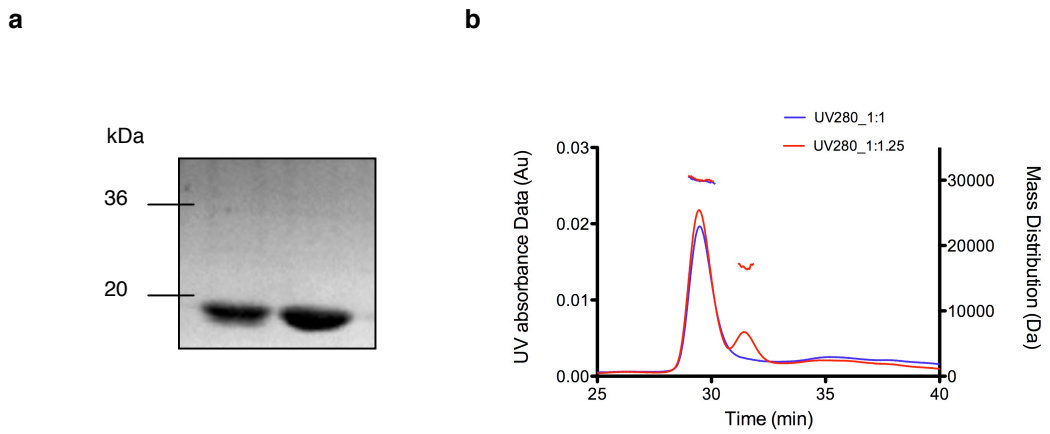

Supplementary Figure 1. SDS-PAGE and Gel filtration analysis of OspE and OspE:FH1920 complex respectively **a.** Coomassie stain of SDS-PAGE gel with OspE used in the NMR-studies (right lane) compared to previously described OspE (left lane) used for X-ray crystallization studies. Mobility of the molecular weight markers is indicated. **b.** The 280 nm spectrum of the OspE:FH1920 complex mixed in 1:1 molar ratio(blue) and OspE:FH1920 complex mixed in 1:1.25 molar ratio (red) on a gel filtration coloumn. The mass distribution of the peaks detected by the matrix assisted laser spectroscopy (MALS) are also plotted on the same timeframe against the right Y-axis.

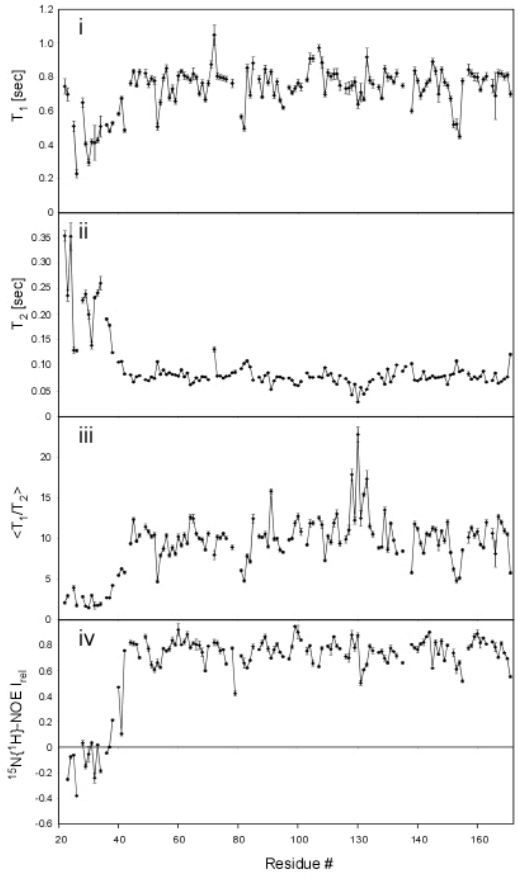

Supplementary Figure 2. The OspE ^{15}N relaxation data. (i) $T_1(^{15}N)$ and (ii) $T_2(^{15}N)$, (iii) T_1/T_2 ratio, and (iv) $^{15}N(1)$-NOE are plotted against the respective residue nos

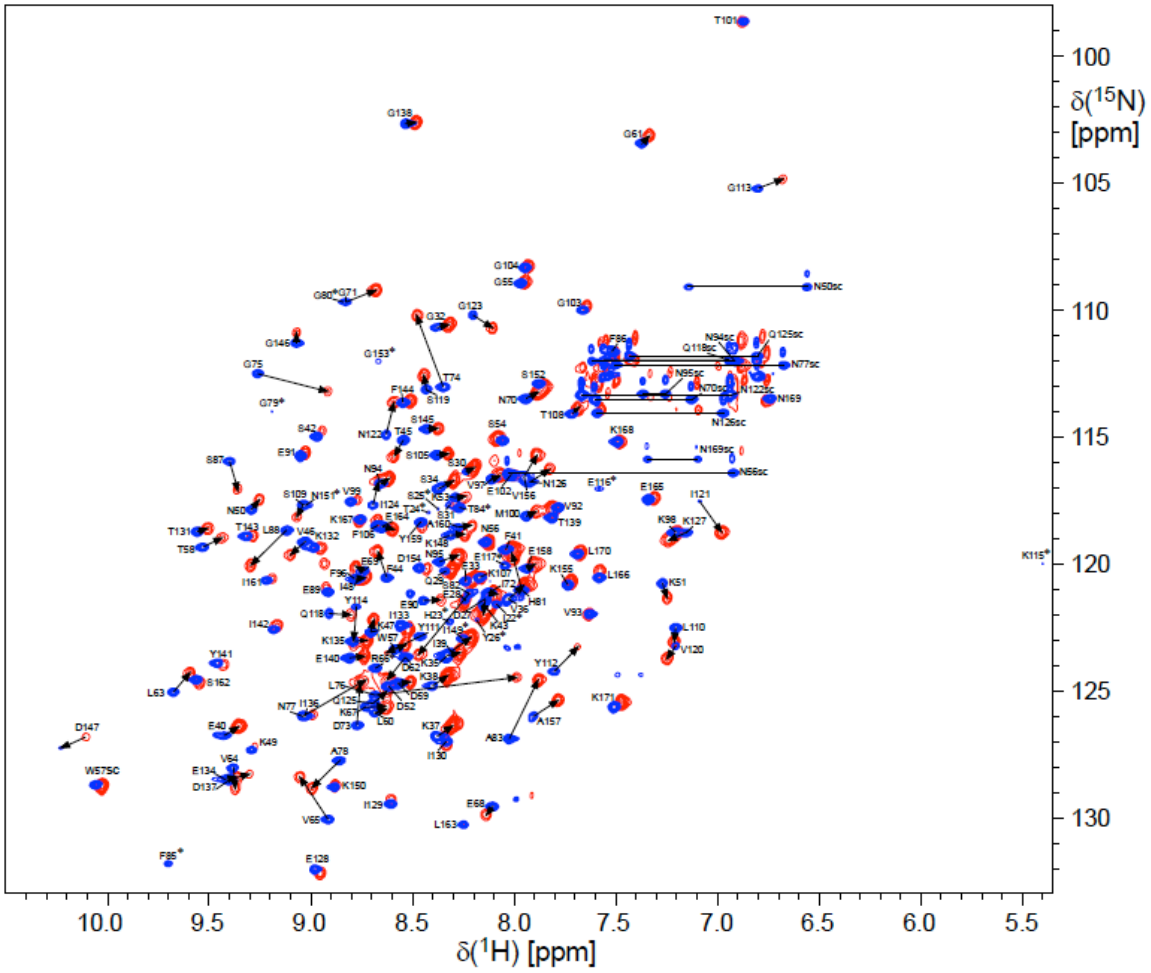

Supplementary Figure 3. ^{15}N-HSQC spectrum of OspE alone (blue) and TROSY ^{15}N-HSQC of OspE saturated with wild type FH19-20 (red). Both spectra are recorded at ^{1}H frequency of 800 MHz. OspE residues with a change in chemical shift upon binding to FH19-20 are indicated with an arrow. Side chain assignments are indicated with 'sc' and the asparagines and glutamine amide side chains are connected with horizontal lines. Residues not assigned in the OspE-FH1920 complex are marked with asterisks.

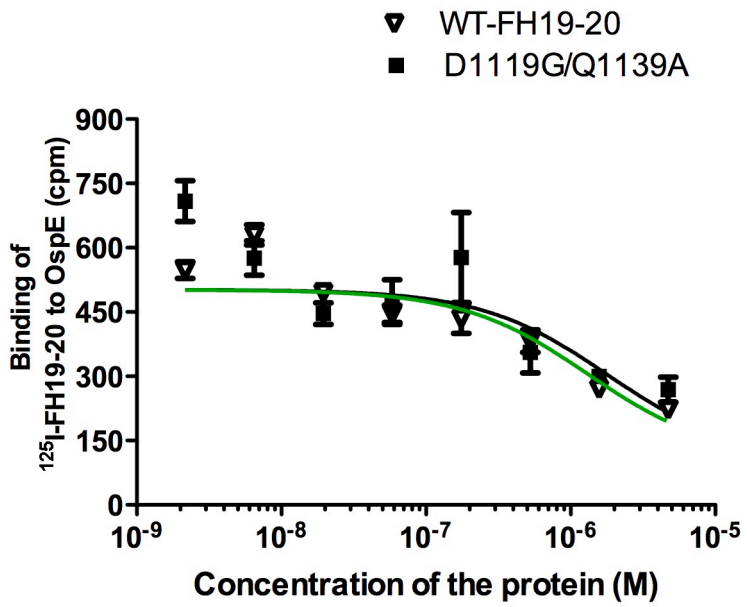

Supplementary Figure 4. Binding studies of wild type FH19-20 and the FH19-20$_{D1119G,Q1139A}$ mutant to OspE. OspE was coated to microtitre plates and the inhibition of the binding of ^{125}I-FH19-20 by the wildtype FH19-20 (green) and the FH19-20$_{D1119G,Q1139A}$ mutant (black) was measured and the data was fitted to inhibition curves. The experiments were performed in triplicates and the SDs are also shown.

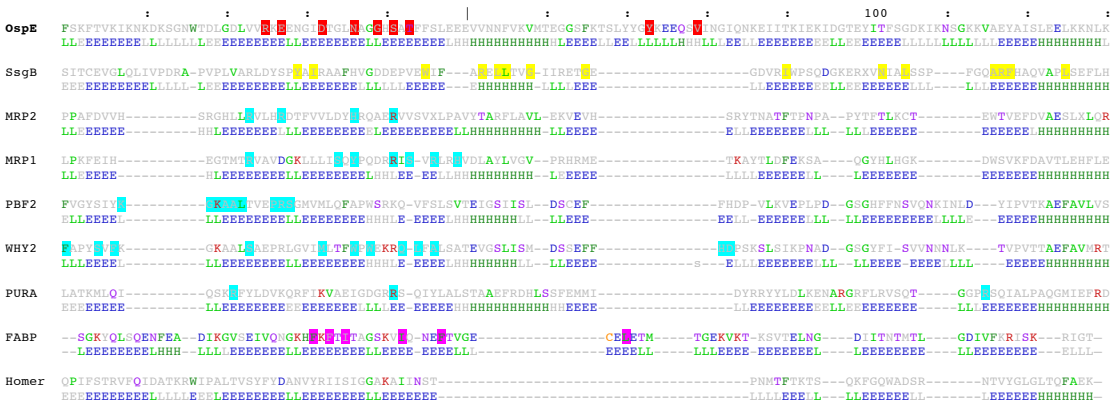

Supplementary Figure 5. A DALI based (See methods) alignment (sequence and secondary structure) of the different OspE structural homologues identified by DALI. Sequence alignment of the OspE and other structural homologues of OspE with color-coded residues. The secondary structure of OspE and other structural homologues of OspE (Codes: H=Helix, E=Sheet, and L=Loop) are mentioned below the sequence. The FH binding residues of OspE are marked with a red background. The functionally important residues of SsgB are marked with a yellow background. The Nucleic acid binding residues of the Nucleic acid binding proteins are marked with an turquoise background. The Fatty acid binding residues of the Fatty acid binding proteins are marked with a magenta background.

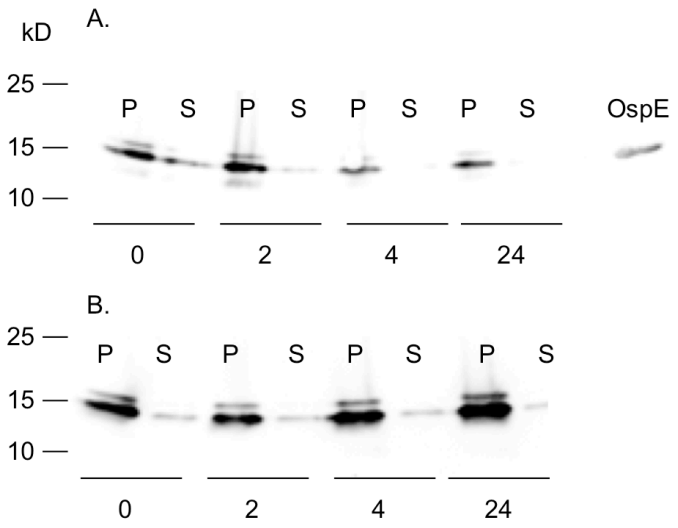

Supplementary Figure 6. Release of OspE from *B. burgdorferi* s.s. (strain N40). Bacteria ($5x10^8$/assay) were incubated in PBS with (panel B) and without (panel A) protease inhibitors. Samples were taken in the beginning, after 2, 4, and 24 hours of incubation (times indicated on the panels below lanes). Bacteria were centrifuged down, and OspE in the pellet (marked with P) and on the supernatant (marked with S) were detected using anti-OspE antibody. As a control purified OspE is shown on the upper membrane. Molecular weight standards are shown on right. OspE is found mainly in the pellets and the small portion of OspE in the supernatant did not increase over time during the incubation.

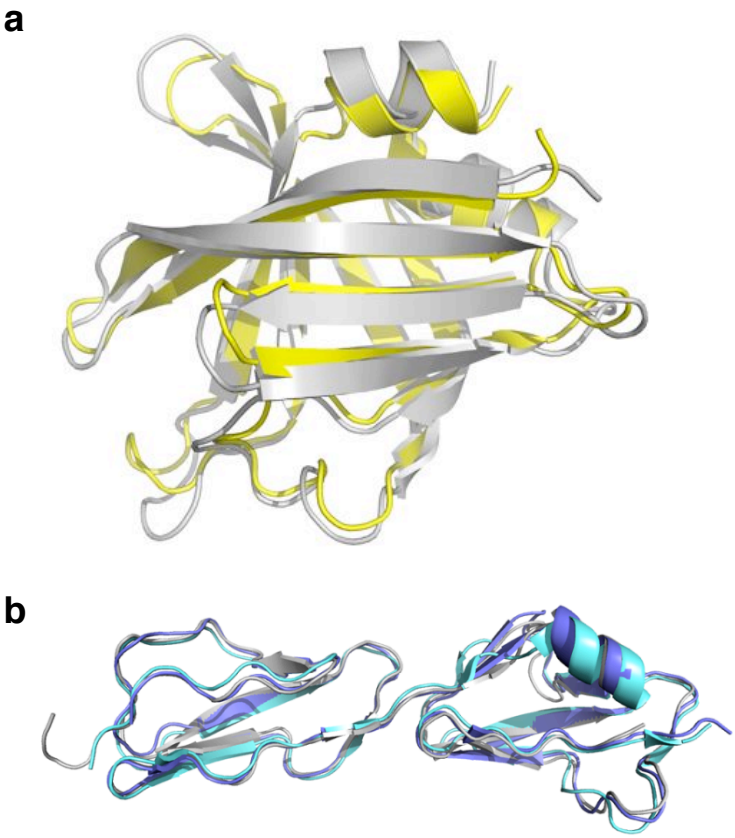

Supplementary Figure 7. Structural alignment of the different OspE and FH19-20 structures. **(a),** Cartoon representation of superimposition of OspE structures obtained with NMR spectroscopy (yellow) and X-ray crystallography (grey). **(b),** Cartoon representation of the three aligned crystal structures of FH19-20: the nonliganded(2) structure shown in turquoise, the structure in complex with OspE shown in grey (this study), and the structure in complex with C3d(3) shown in blue.

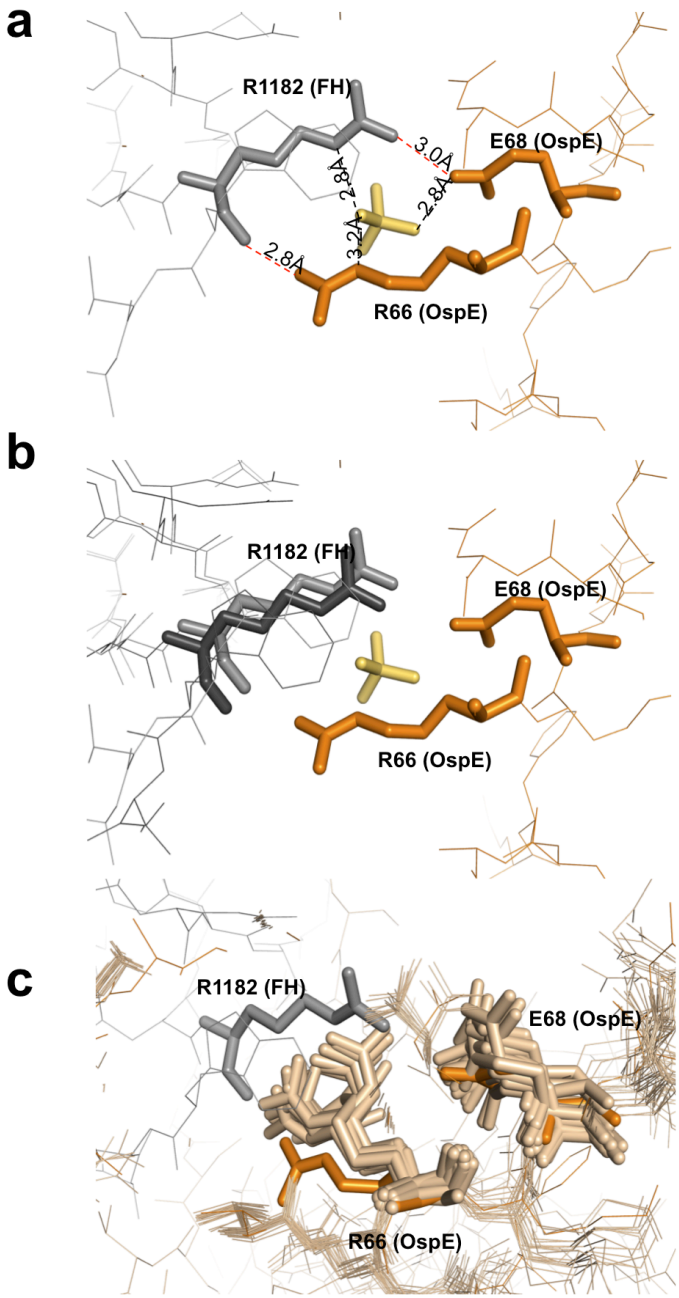

Supplementary Figure 8. Close view of the SO4 ion in the FH19-20:OspE complex. **(a)**, View of the SO4 ion with the hydrogen bonds being formed by it with the adjacent residues from OspE (ochre) and FH (gray). The interprotein hydrogen bonds are shown in red. **(b)**, Superimposition of previously solved FH19-20 structure (with no sulphate ions in this region, 2G7I, dark grey) on FH19-20 of the complex structure. **C**, Superimposition of the NMR ensemble of OspE (wheat) on the OspE in the complex structure (ochre).

Supplementary references

1. Farrow, N. A., Muhandiram, R., Singer, A. U., Pascal, S. M., Kay, C. M., Gish, G., Shoelson, S. E., Pawson, T., Forman-Kay, J. D., and Kay, L. E. (1994) *Biochemistry* **33**, 5984-6003
2. Jokiranta, T. S., Jaakola, V. P., Lehtinen, M. J., Parepalo, M., Meri, S., and Goldman, A. (2006) *EMBO J* **25**, 1784-1794
3. Kajander, T., Lehtinen, M. J., Hyvarinen, S., Bhattacharjee, A., Leung, E., Isenman, D. E., Meri, S., Goldman, A., and Jokiranta, T. S. (2011) *Proc Natl Acad Sci U S A* **108**, 2897-2902